Magnetoelectric effect at the $Fe_3O_4/BaTiO_3$ (001) interface: A first-principles study

Manish K. Niranjan,[1,*] Julian P. Velev,[1] Chun-Gang Duan,[2] S. S. Jaswal,[1] and Evgeny Y. Tsymbal[1,†]
[1]*Department of Physics and Astronomy and Nebraska Center for Materials and Nanoscience, University of Nebraska, Lincoln, Nebraska 68588, USA*
[2]*Key Laboratory of Polarized Materials and Devices, Ministry of Education, East China Normal University, Shanghai 200062, People's Republic of China*
(Received 1 May 2008; published 11 September 2008)

Multiferroic heterostructures comprising ferroelectric and ferro(ferri)magnetic constituents have recently attracted considerable interest due to the strong coupling between magnetic and electric properties which may have interesting applications. Here we investigate the magnetoelectric coupling at the ferrimagnetic/ferroelectric $Fe_3O_4/BaTiO_3(001)$ interfaces within the framework of density-functional theory. The coupling in this system originates from the interface bonding sensitive to atomic displacements at the interface and leads to the change in the interface magnetization when the polarization of the ferroelectric layer reverses. We consider two types of interface terminations of Fe_3O_4 which have different iron cation valence and oxygen atom environment. We find that the magnitude of the magnetoelectric coupling is stronger for the oxygen-deficient $Fe_3O_4/BaTiO_3(001)$ interface. The sensitivity to the interface oxygen content suggests that oxidation or oxygen vacancies at the interface may play an important role in determining the strength of the interface magnetoelectric coupling.

DOI: 10.1103/PhysRevB.78.104405 PACS number(s): 75.70.Cn, 75.70.Ak, 75.80.+q

I. INTRODUCTION

Multiferroic materials have recently attracted much scientific interest due to enhanced and unconventional magnetoelectric (ME) coupling between ferroelectricity and ferromagnetism.[1–3] The coupling in such materials allows the electric control of magnetic polarization[4] and the magnetic control of electric polarization.[5] In a broader vision, magnetoelectric effects include not only the coupling between the order parameters, but also involve related phenomena such as an electrically controlled exchange bias,[6,7] electrically controlled magnetocrystalline anisotropy,[8–11] and the effect of ferroelectricity on spin transport.[12–16] Tailoring the magnetization, exchange bias, and magnetic anisotropy by electric fields opens unexplored avenues for device applications of magnetoelectric heterostructures.

There are two major sources of magnetoelectric coupling. An intrinsic ME coupling occurs in compounds in which time-reversal and space-inversion symmetries are absent. In such materials, an external electric field displaces the magnetic ions, eventually changing the exchange interactions between them and hence the magnetic properties of the compound.[17] A reverse effect is observed when an external magnetic field is applied. A different mechanism of ME coupling may occur in composites of piezoelectric (ferroelectric) and magnetostrictive (ferro- or ferrimagnetic) compounds. In such structures the coupling is mediated by strain across interfaces. Here, an applied electric field induces strain in the piezoelectric constituent which is mechanically transferred to the magnetostrictive constituent where it induces a magnetization. In recent years, composite multiferroics have been intensively studied.[9,18–23] Such composites can be fabricated in the form of multilayers of alternating ferroelectric and ferro(ferri)magnetic layers[9,10] or vertically aligned columnar nanostructures.[18,19] The importance of composite multiferroics follows from the fact that none of the existing single phase multiferroic materials combine large and robust electric and magnetic polarizations at room temperature.[1–3]

In addition to aforementioned mechanisms of ME coupling, two other mechanisms have recently been proposed based on theoretical studies.[24,25] In both cases the ME coupling is confined to the interface of the composite constituents. Duan *et al.*[24] demonstrated that the interface bonding may be the source of the interface ME effect. Using $Fe/BaTiO_3(001)$ multilayer as a representative model they showed that atomic displacements at the interface caused by ferroelectric switching change the overlap between atomic orbitals at the interface that affects the interface magnetization. A similar effect was recently found for $Co_2MnSi/BaTiO_3$ interface.[26] Another kind of the interface ME effect has been predicted by Rondinelli *et al.*[25] They found that the ME effect may be mediated by free carriers at the interface between a nonmagnetic, nonpolar insulator and a ferromagnetic metal. In this case, an electric field results in the accumulation of spin-polarized carriers at the metal-insulator interface producing a change in the interface magnetization.

The previous studies of the interface ME effect in $Fe/BaTiO_3(001)$ system[24] found the induced magnetic moment of about 0.3 μ_B on the interfacial Ti atoms due to the overlap between Ti and magnetic Fe orbitals. Ferroelectric displacements cause magnetic moments of Ti and Fe atoms at the interfaces to deviate from their values in the paraelectric state. Differences of about 0.1 and 0.2 μ_B in the magnetic moments of Fe and Ti atoms, respectively, were found for the two opposite polarization orientations in $BaTiO_3$ indicating a large ME effect. The predicted phenomenon is qualitatively different from the "standard" magnetoelectric effect which is the volume effect and for which the magnetization is a linear function of the applied electric field. In this case the magnetoelectric effect is confined to the interface and represents a change of the interface magnetization at the coercive field of the ferroelectric. These results are

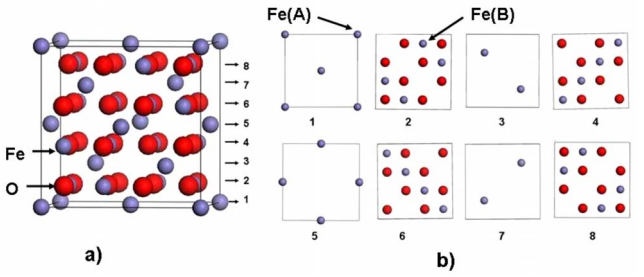

FIG. 1. (Color online) Atomic structure of bulk Fe_3O_4: (a) Cubic unit cell of Fe_3O_4; (b) plane by plane (001) structure of Fe_3O_4. Planes numbered as 1, 3, 5, 7 and 2, 4, 6, 8 designate Fe(*A*) and Fe(*B*)O_2 planes, respectively. Blue and red circles indicate Fe and O atoms.

very promising, demonstrating new kind of ME phenomenon which has potential for multifunctional device applications. However, growth of high quality Fe films on $BaTO_3$ films resulting in the epitaxial Fe/$BaTiO_3$(001) interface may be challenging due to possible oxidation of the Fe film.

In this article, we consider magnetite (Fe_3O_4) as a magnetic material to avoid the oxidation problem. Magnetite is a ferrimagnet and has interesting magnetic and transport properties. Besides having been used for thousands of years as a magnetic material in compasses, in recent years it has become a potential candidate for spintronics and magnetoelectric devices.[27–31] Interestingly, at low temperatures, Fe_3O_4 becomes magnetoelectric[32] and shows a magnetically addressable small polarization as well.[33] Here we investigate the interface magnetoelectric coupling in Fe_3O_4/$BaTiO_3$(001) heterostructure using density-functional theory. This choice of materials is also motivated by the recent experimental studies showing the possibility of epitaxial growth of high quality Fe_3O_4 thin films on ferroelectric $BaTiO_3$.[23] By considering two different interface terminations of Fe_3O_4, we explore the effect of oxygen atom environment on the magnitude of the ME effect.

The rest of the paper is organized as follows: In Sec. II, we present the calculation methodology and discuss the electronic and atomic structures of the bulk Fe_3O_4 and Fe_3O_4/$BaTiO_3$(001) interfaces. In Sec. III we study the effect of interfacial atomic bonding and ferroelectric switching on the magnetization at the interface using the details of the electronic structure of the interface. Concluding remarks are given in Sec. IV.

II. CALCULATION METHODOLOGY AND INTERFACE MODEL

At room temperature bulk Fe_3O_4 (magnetite) crystallizes in the inverted cubic spinel structure (space group $Fd3m$) and has chemical formula $[Fe(\downarrow)]_A[Fe_2(\uparrow)]_BO_4$ as shown in Fig. 1(a). Figure 1(b) shows the layer by layer structure of Fe_3O_4. There are two distinct Fe cation sites: tetrahedron *A* sites and octahedron *B* sites. Fe atoms in the two sites have magnetic moments oriented in the opposite directions, as indicated by arrows in the chemical formula given above. In the ionic picture, the *A* sites are occupied by Fe^{3+} cations, whereas *B* sites are occupied by an equal number of randomly distributed Fe^{2+} and Fe^{3+} cations. Alternatively, one can also envisage the extra electron hopping on *B* sites Fe^{3+} cations giving rise to conducting states at the Fermi level. Magnetite is a ferrimagnet with an anomalously high critical temperature of 860 K. The ferrimagnetic ordering arises due to the strong antiferromagnetic coupling between Fe cations on *A* and *B* sublattices. The Fe cations are coupled ferromagnetically within the *B* sublattice. At room temperature, magnetite is a poor metal. It undergoes a first-order metal-insulator (Verway) transition at 120 K with crystal structure changing from cubic to monoclinic.[34] The physical mechanism of the Verway transition is still a subject of debate.[35–37]

We use density-functional theory[38] (DFT) with the projected augmented wave (PAW) method,[39] as implemented within Vienna *Ab-Initio* Simulation Package (VASP).[40] The Perdew-Burke-Ernzerhoff[41] (PBE) form of the generalized gradient approximation (GGA) for exchange and correlation is employed along with a standard plane-wave basis set with a kinetic-energy cutoff of 520 eV. The bulk calculations are performed using the $8\times8\times8$ Monkhorst-Pack[42] *k*-point mesh for the $BaTiO_3$ and Fe_3O_4. The calculations are converged to 10^{-4} eV/cell and the structures are relaxed until the largest force becomes less than 0.04 eV/Å.

Experimental and calculated values of the lattice constant, magnetic moment per formula unit, and magnetic moments of Fe(*A*) and Fe(*B*) ions in Fe_3O_4 are presented in Table I. The calculated lattice constant 8.391 Å is in excellent agreement with the reported experimental value 8.394 Å.[43] Figure 2(a) shows the total density of states of Fe_3O_4, and Figs. 2(b) and 2(c) show the partial density of states projected onto Fe octahedron *B* sites and tetrahedron *A* sites. As evident from Fig. 2(a), the Fermi level lies in the band gap of the majority-spin channel, rendering the magnetite a half metal. Further, it is clear from Figs. 2(b) and 2(c) that the conducting states at the Fermi level are derived predominantly from 3*d* orbitals of Fe cations at the octahedron *B* sites. The results are consistent with the previous theoretical work.[44]

We note, however, that the half metallic behavior of magnetite has not been established experimentally. In particular, the electronic band structure of Fe_3O_4 has been investigated extensively using photoelectron spectroscopy techniques (see, e.g., Ref. 45). The interpretation of valence-band photoemission spectra is still a matter of debate. Spin polarization up to 80% has been measured on Fe_3O_4(111) surface as compared to band theory prediction of 100%. We note that the photoemission data include a contribution from the surface electronic structure which may not have half metallic properties. Indeed, DFT study of Fe_3O_4 (100) surface shows significant reduction of the spin polarization at the Fermi level compared to the bulk density of states suggesting the role of surface states in reduction of spin-polarization value.[45] Another mechanism which may lead to the deviation from the half metallic behavior is the admixture of minority-spin states and the "insulating" majority-spin states due to noncollinear spin moments at elevated temperatures.[46]

The nature and degree of electronic correlations in magnetite is another issue which remains under study. It is believed that at temperatures below the Verwey transition, where the magnetite is in the insulating state, the on-site

TABLE I. Theoretical and experimental values of lattice constants (in Å), magnetic moments per formula unit (in μ_B), and electric polarizations (in C/m^2).

Material			a (Å)	c/a	Magn. mom. (μ_B)	Polar. (C/m^2)
Fe_3O_4	Bulk	Calc.	8.391		4.00	
		exp.[a]	8.394		4.07	
	Fe(A)	calc.			−3.47	
	Fe(B)	calc.			3.56	
	O	calc.			0.08	
Fe_3O_4	Strained	calc.	8.06	1.08	4.00	
	Fe(A)	calc.			−3.38	
	Fe(B)	calc.			3.50	
	O	calc.			0.08	
$BaTiO_3$		calc.	4.03			0.33
		exp.	4.01			0.30

[a]Reference 43.

Coulomb interaction plays an important role and has to be taken into account.[47–49] We have studied the electronic structure of room-temperature cubic phase of bulk magnetite within the local spin-density approximation (LSDA) and LSDA plus on-site Coulomb interaction (the LSDA+U method[50]). We do not find any significant changes in the magnetization of magnetite with LSDA+U except for an enhanced gap in the density of states for majority-spin electrons. Also it has been shown in Ref. 45 that LSDA calculations are in very good agreement with the photoemission data for Fe_3O_4. Due to these successes of the LSDA, we feel that it is reasonable for the magnetization related studies carried out in this paper.

The $Fe_3O_4/BaTiO_3(001)$ interface is simulated by building up supercells consisting of Fe_3O_4 (001) layers on top of $BaTiO_3$ (001) layers. The (001) film orientation is consistent with the recently performed experimental work.[23] We assume that $BaTiO_3$ serves as a substrate for Fe_3O_4 film. Therefore, the lateral in-plane lattice constants of epitaxial Fe_3O_4 are strained by −3.8% to match twice the calculated bulk $BaTiO_3$ lattice constant (see Table I). The resulting compressive strain in the Fe_3O_4 film is accommodated by elongation along the out-of-plane lattice constant in the growth direction. The corresponding out-of-plane lattice constant of Fe_3O_4 is calculated by minimizing the total energy of the appropriately strained Fe_3O_4 unit cell. Lattice constants, magnetic moment per formula unit, and magnetic moments of Fe(A) and Fe(B) ions in the strained bulk Fe_3O_4 are presented in Table I. It is seen that the in-plane compression results in small changes in the local magnetic moments. Densities of states of the strained bulk Fe_3O_4 are similar to those of the unstrained Fe_3O_4 shown in Fig. 2.

The supercells are constructed of six unit cells (12 monolayers) of $BaTiO_3$ (001) with one unit cell (8 monolayers) of Fe_3O_4 (001) on top in epitaxial arrangement, as shown in Fig. 3(a). We chose TiO_2 surface termination of $BaTiO_3$ (001) and Fe(A) and FeO_2(B) surface terminations of Fe_3O_4 (001) at the interface. The TiO_2-terminated surface of $BaTiO_3$ has been found more energetically favorable over BaO-terminated surface in the previous study of $Fe/BaTiO_3$

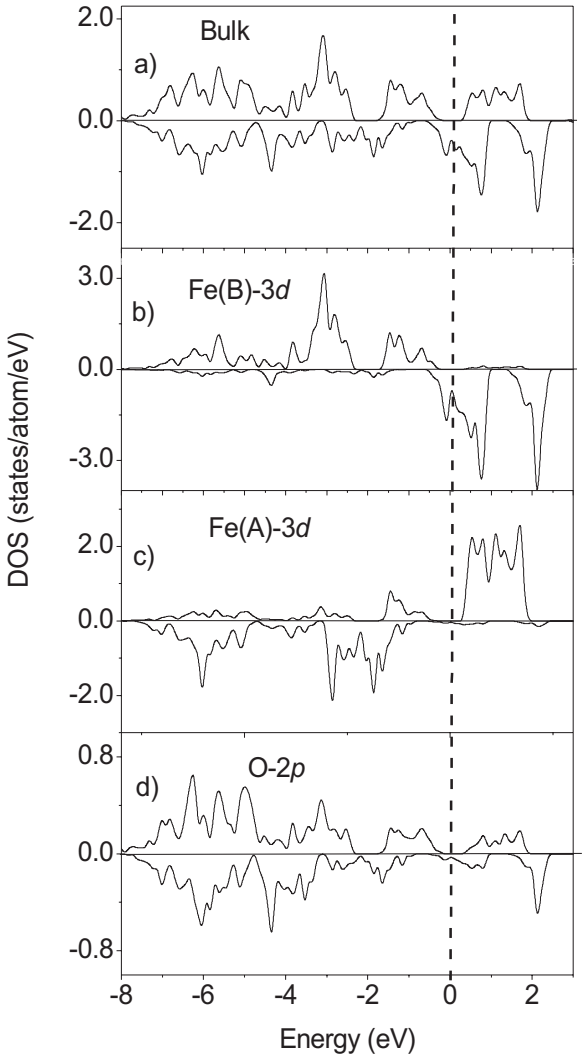

FIG. 2. Density of states (DOS) of bulk Fe_3O_4: (a) The total DOS; (b) DOS projected onto the Fe d orbitals at octahedron B sites; (c) DOS projected onto the Fe d orbitals at tetrahedron A sites; (d) DOS projected onto the O p orbitals at octahedron sites. The Fermi energy is indicated by the dashed line.

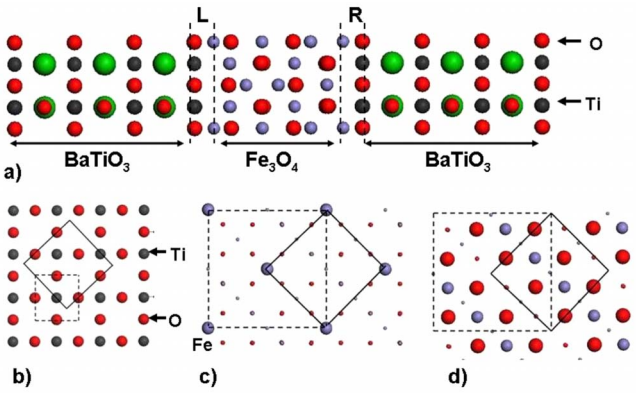

FIG. 3. (Color online) The atomic structure of $BaTiO_3/Fe_3O_4(001)$: (a) Supercell structure with TiO_2-Fe(A) interface. The in-plane lattice constant is $\sqrt{2}$ times lattice constant of bulk $BaTiO_3$. L and R indicate left and right interfaces. (b) Top view of the $(\sqrt{2}\times\sqrt{2})R45°$ surface unit cell of TiO_2-terminated $BaTiO_3(001)$ surface as indicated by bold lines. 1×1 surface unit cell is shown by a dashed line. (c) Top view of surface unit cell of Fe(A)-terminated $Fe_3O_4(001)$ interface as indicated by bold lines. The dashed line shows the surface unit cell of cubic Fe_3O_4. Small circles are Fe and O atoms on lower layers. (d) Top view of the surface unit cell of FeO_2(B)-terminated $Fe_3O_4(001)$ surface as indicated by bold lines. The dashed line shows the surface unit cell of cubic Fe_3O_4. Small circles are Fe and O atoms on lower layers.

heterostructures[24] (see also Ref. 51). The surface unit cell of TiO_2-terminated $BaTiO_3(001)$ has $(\sqrt{2}\times\sqrt{2})R45°$ periodicity and contains two Ti atoms and four O atoms as shown in Fig. 3(b). We consider two different interface terminations of Fe_3O_4. The Fe(A)-terminated surface contains Fe cations on tetrahedron A sites, whereas FeO_2(B)-terminated surface contains Fe cations on octahedron B sites in addition to O anions. Figures 3(c) and 3(d) show the surface unit cells of Fe(A) and FeO_2(B)-terminated $Fe_3O_4(001)$ surfaces at the $Fe_3O_4/BaTiO_3(001)$ interfaces. Density-functional calculations of the electronic and anomic structure for the $Fe_3O_4/BaTiO_3(001)$ superlattice are performed using $6\times6\times1$ Monkhorst-Pack mesh of k points in the Brillouin zone.

III. MAGNETOELECTRIC COUPLING

Here we calculate and analyze induced magnetic moments on the interfacial atoms and the resulting change of these moments due to electric polarization reversal in the ferroelectric $BaTiO_3$ film. This change determines the interface magnetoelectric effect.

The total energy of the $Fe_3O_4/BaTiO_3(001)$ structure with respect to the cell size and atomic coordinates of all the atoms is minimized using the procedure as follows: First, the length of the supercell along the z direction, normal to the planes, is determined by varying the interplanar distances keeping the in-plane lattice constants fixed. Afterwards, the total energy of the supercell is minimized with respect to all the atomic coordinates keeping all the lattice constants unchanged. For the six unit-cell $BaTiO_3$ film, the minimum-energy structure demonstrates the presence of a nonzero ferroelectric polarization in the $BaTiO_3$. Relative displacements of Ti atoms with respect to O atoms in the middle of $BaTiO_3$ film are found to be about 0.10 Å. These values are close to the bulk values of 0.11 Å which correspond to the calculated polarization of 0.33 C/m^2 of the bulk $BaTiO_3$.

TABLE II. Magnetic moments of Ti, O, and Fe atoms at the TiO_2-Fe(A) interface (in units of μ_B) for electric polarization pointing left to right (μ_1) and right to left (μ_2) in Fig. 3(a).

Interface	Atom	μ_1	μ_2	$\Delta\mu(\mu_1-\mu_2)$
	Ti	0.13	−0.05	0.18
	Ti	0.35	0.02	0.33
Left	O	0.01	0.01	0.00
	O	0.01	0.01	0.00
	O	−0.10	−0.11	0.01
	O	−0.10	−0.11	0.01
	Ti	−0.03	0.16	−0.19
	Ti	0.20	0.38	−0.18
Right	O	−0.10	−0.10	0.00
	O	−0.10	−0.10	0.00
	O	0.03	0.02	0.01
	O	0.03	0.02	0.01
Left	Fe	−3.35	−3.53	0.18
Right	Fe	−3.36	−3.30	−0.06

We note that reducing the $BaTiO_3$ film thickness below six unit cells leads to the quenching of the ferroelectric state. This result is different from the previous findings showing that the critical thickness for ferroelectricity can be as small as one to three unit cells of the thin film.[24,52–56] We attribute this difference to the interface bonding which in the case of $Fe_3O_4/BaTiO_3(001)$ is rather strong resulting in pinning the positions of the interface atoms which is detrimental to the formation of the soft mode in the ferroelectric film.[55] Also screening of the polarization charges by Fe_3O_4 is not as strong as that by normal metals such as Fe leading to the increased critical thickness of $BaTiO_3$.

The calculations find induced magnetic moments on Ti and O atoms and modified magnetic moments on Fe atoms at the left and right interfaces as compared to the bulk. The magnitude of these moments depends on polarization orientation in the $BaTiO_3$ film. First we discuss the TiO_2-Fe(A) interface shown in Figs. 3(a)–3(c). Table II presents the magnetic moments on Ti, O, and Fe atoms for two polarization states. The polarization pointing to right corresponds to Ti atoms displaced to the right with respect to O atoms in $BaTiO_3$ and polarization pointing to left corresponds to Ti atoms displaced to the left with respect to O atoms. The induced magnetic moments on two Ti atoms at the interface are 0.33 and 0.13 μ_B when the polarization is pointing right. However, the magnetic moments are reduced to −0.05 and 0.02 μ_B as the electric polarization of the ferroelectric is reversed. The difference in magnetic moments for two Ti atoms at the left interface caused by polarization reversal is

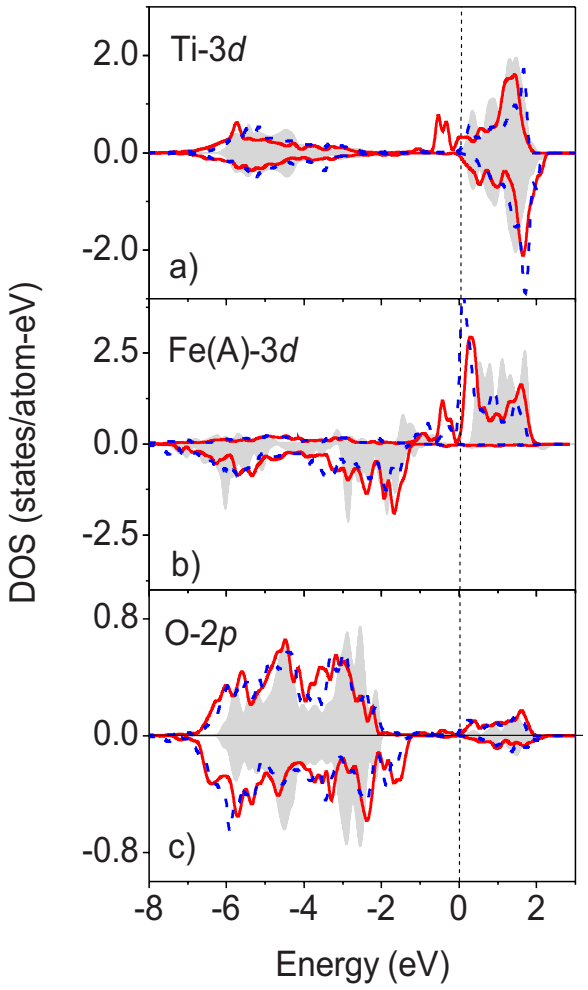

FIG. 4. (Color online) Density of states (DOS) at the left Fe(A)-terminated interface of $BaTiO_3/Fe_3O_4(001)$: (a) DOS projected on the Ti 3d orbitals; (b) DOS projected on the Fe(A) 3d orbitals; (c) DOS projected on the O 2p orbitals. Solid and dashed lines denote DOS for electric polarization pointing right and left, respectively. Shaded plots are the DOS projected on Fe(A)3d orbitals in the central monolayer of Fe_3O_4 (b) and on Ti 3d orbitals (a) and O 2p orbitals in the central TiO_2 monolayer of $BaTiO_3$ which can be regarded as bulk. The vertical line indicates the Fermi energy.

therefore $\Delta\mu=0.33$ and 0.18 μ_B. The induced magnetic moments on O atoms are sizeable (of about 0.1 μ_B) though the net change under polarization reversal is negligible. The difference in magnetic moments of interface Fe atom is $\Delta\mu=0.18$ μ_B. Total change in the magnetic moment per surface cell is about 0.6 μ_B. We have verified the convergence of the results by studying heterostructures composed of six unit cells (12 monolayers) of $BaTiO_3$ and two unit cells (16 monolayers) of Fe_3O_4. The observed changes in the magnetic moments and their differences for two ferroelectric polarization cases are obtained to be less than 7%.

The origin of the induced magnetic moments at the interface and their change with polarization orientation can be understood from the site and orbital projected density of states (DOS) shown in Fig. 4. As evident from Figs. 4(a) and 4(b), Ti 3d states hybridize with exchange-split Fe 3d states. The hybridization results in the formation of exchange-split Ti 3d bonding and antibonding states, giving rise to induced magnetic moment on Ti atoms. We note that the induced Ti magnetic moments are aligned antiparallel to Fe(A) magnetic moment (Table II). As seen from Figs. 4(a) and 4(b), the Ti 3d band is centered approximately 2 eV above the Fermi energy and overlaps strongly with the minority-spin Fe 3d band which is peaked at these energies. The bonding states are created by the hybridization between the Fe and Ti 3d orbitals and lie just below the Fermi energy. This implies an induced magnetic moment on Ti atom is aligned antiparallel to the magnetic moment of Fe(A) atom.

When the electric polarization reverses, exchange-split Ti-Fe(A)3d bonding states are reduced significantly, as is evident from Fig. 4(a). This leads to the reduction of the induced magnetic moments on Ti atoms from 0.35 and 0.13 μ_B to 0.02 and −0.05 μ_B at the left interface (see Fig. 3(a) and Table I). The electric polarization reversal makes the Ti atoms (at the left interface) move away from the interfacial Fe(A) atoms resulting in an increase in Ti-Fe(A) bond lengths from 2.45 and 3.27 Å to 2.64 and 3.45 Å, respectively, which reduces the overlap between Ti 3d and Fe(A)3d states and, hence, the hybridization between them.

Changes at the right interface with polarization reversal are similar to those observed at the left interface. This is seen from Table II which shows the magnetic moments of Ti, Fe, and O atoms at the right interface. The difference originates from the fact that the considered unit cell does not have the reflection symmetry in the *paraelectric* state of $BaTiO_3$. This means that, for the *ferroelectric* state on $BaTiO_3$, the simultaneous reversal of the polarization and mirror reflection of the supercell structure does not produce the identity transformation.

Next, we study TiO_2-FeO_2(B) interface. The TiO_2(001) and FeO_2(B) (001) surfaces at the interface are shown in Figs. 3(b) and 3(d). The magnetic moments on Ti, O, and Fe atoms at the left and right interfaces for two electric polarization states (right or left) are presented in Table III. As seen from this table, the induced magnetic moments on Ti atoms at the left interface are −0.05 and −0.06 μ_B when the electric polarization is pointing right and −0.01 μ_B when the electric polarization is switched to left. The resulting difference in magnetic moments of Ti atoms at the left interface caused by polarization reversal is $\Delta\mu=-0.05$ μ_B. The smaller induced magnetic moments and smaller changes in the moments with polarization reversal as compared to the TiO_2-Fe(A) interface can be explained by larger bond lengths and their smaller change under polarization reversal. The Ti-Fe(B) bond length at the TiO_2-Fe(B) interface is about 2.90 Å and changes by about 0.06 Å [compared to 0.2 Å at the TiO_2-Fe(A) interface] when polarization reverses. The induced magnetic moments on O atoms on TiO_2 and FeO_2 surfaces are sizeable and higher than those on Ti atoms. However, the net change in the O magnetic moments under polarization reversal is very small. The difference in the magnetic moments of interface Fe atoms as the polarization is reversed is $\Delta\mu=0.05$ μ_B. Table III also shows the magnetic moments of Ti, Fe, and O atoms at the right interface. We further note that the induced magnetic moments on Ti atoms and the difference caused due to polarization reversal

TABLE III. Magnetic moments of Ti, O, and Fe atoms at the TiO_2-$FeO_2(B)$ interface (in units of μ_B) for electric polarization pointing left to right (μ_1) and right to left (μ_2) in Fig. 3(a).

Interface	Atom	μ_1	μ_2	$\Delta\mu(\mu_1-\mu_2)$
	Ti	−0.06	−0.01	−0.05
	Ti	−0.05	−0.01	−0.04
Left	O	0.12	0.14	−0.02
	O	0.10	0.12	−0.02
	O	0.00	0.00	0.00
	O	0.01	0.01	0.00
	Ti	−0.01	−0.05	0.04
	Ti	−0.01	−0.05	0.04
Right	O	0.14	0.12	0.02
	O	0.12	0.10	0.02
	O	0.01	0.01	0.00
	O	0.01	0.01	0.00
	Fe	3.66	3.71	−0.05
	Fe	3.65	3.70	−0.05
Left	O	0.02	0.03	−0.01
	O	0.02	0.02	0.00
	O	0.23	0.25	−0.02
	O	0.25	0.26	−0.01
	Fe	3.70	3.65	0.05
	Fe	3.69	3.64	0.05
Right	O	0.25	0.23	0.02
	O	0.26	0.25	0.01
	O	0.03	0.04	−0.01
	O	0.04	0.03	0.01

are smaller for the TiO_2-$FeO_2(B)$ interface than those for the TiO_2-$Fe(A)$ interface. The total change in the magnetic moment per surface cell for the TiO_2-$FeO_2(B)$ interface is about 0.2 μ_B.

We see therefore that for both interface terminations magnetic moments of the atoms at the interface undergo a change as the polarization of the ferroelectric reverses. Bulk magnetoelectric properties of materials are quantified using a bulk magnetoelectric coefficient which links the electric field and the induced magnetization.[1] For not too large electric fields this relationship is linear. In our case the magnetoelectric effect is confined to the interface and the relationship is nonlinear because the interface magnetization depends on the ferroelectric polarization which is nonlinear function of an applied electric field. Nevertheless, to have an estimate of the strength of the interface ME effect we use a linear relationship introduced in Ref. 57 between the induced interface magnetization ΔM and the applied electric field E:

$$\mu_0 \Delta M = \alpha_s E.$$

Here α_s is *the surface magnetoelectric coefficient*. To make the estimate we assume that the polarization of $BaTiO_3$ can be switched at the coercive field of $E=E_c=100$ kV/cm resulting in the change of the interface magnetic moment of $\sim 0.6\ \mu_B$ per unit surface cell corresponding to the TiO_2-$Fe(A)$ interface. We find that the interface magnetoelectric coefficient is then $\alpha_s \approx 2.1\times 10^{-10}$ G cm^2/V. This is similar to the value of $\approx 2.2\times 10^{-10}$ G cm^2/V found at the $Fe/BaTiO_3$ interface.[24] For the TiO_2-$FeO_2(B)$ interface in the $Fe_3O_4/BaTiO_3$ structure the surface magnetoelectric coefficient is smaller by a factor of three, i.e., $\alpha_s \approx 0.7 \times 10^{-10}$ G cm^2/V.

It is interesting to compare the calculated magnitudes of the surface magnetoelectric coefficient due to the interface bonding mechanism (this work and Duan *et al.*[24]) to that resulting from the carrier mediated mechanism predicted by Rondinelli *et al.*[25] Rondinelli *et al.* found that the magnetoelectric effect may be produced by the spin-dependent screening of the polarization charges at the $SrTiO_3/SrRuO_3$ interface due to the polarization of the $SrTiO_3$ layer induced by an external electric field. The results of the calculations by Rondinelli *et al.* suggest that for a seven unit cell thick $SrTiO_3$ layer (a=3.85 Å) the applied voltage of 27.8 mV induces a net magnetic moment of 2.5×10^{-3} μ_B per surface unit cell. The corresponding magnetoelectric coefficient is therefore $\alpha_s \approx 2\times 10^{-12}$ G cm^2/V. This value is lower by about 2 orders in magnitude compared to those found in this work and by Duan *et al.*[24] This fact indicates that much stronger magnetoelectric effects are expected at the ferroelectric/ferromagnetic interfaces as the result of the change in bonding properties due to ferroelectric displacements.

Finally we would like to emphasize the fact that the predicted magnetoelectric effect is very sensitive to the choice of the interface. We find that the magnetoelectric effect is more pronounced for the case of TiO_2-$Fe(A)$ interface than that of TiO_2-$FeO_2(B)$. As was mentioned earlier in the section, the TiO_2-$FeO_2(B)$ interface has four extra oxygen atoms than TiO_2-$Fe(A)$ interface. These O atoms produce strong bonds with interface Fe atoms reducing the hybridization between Fe and Ti thus decreasing the magnitude of the induced moments on interface Ti atoms. This leads to the reduction of the ME effect since it is primarily controlled by the magnetic moments on Ti atoms sensitive to the Fe-Ti bond length. This fact suggests that the amount of O at the interface may play an important role in determining the magnetoelectric coupling caused by the atomic orbital overlap at the ferroelectric/ferri(ferro)magnetic interfaces. Therefore, the strength of the magnetoelectric coupling may be controlled by the degree of oxidation of the interfaces. Interestingly, oxygen vacancies appear to change significantly surface magnetic properties of Fe_3O_4 as reported in Ref. 58. Our results suggest the possibility to observe a net magnetization and its alteration induced by the ferroelectric polarization in a $Fe_3O_4/BaTiO_3$ composite structure. However, the coupling strength may depend on the interface between two materials, *viz.*, oxygen-rich TiO_2-$FeO_2(B)$ and oxygen-deficient TiO_2-$Fe(A)$.

IV. CONCLUSIONS

We have studied the magnetoelectric coupling at the ferroelectric/ferrimagnetic $Fe_3O_4/BaTiO_3(001)$ interfaces. We find that there are induced magnetic moments on interface Ti and O atoms which are sensitive to ferroelectric displacements in the ferroelectric $BaTiO_3$. The reversal of the ferroelectric polarization in $BaTiO_3$ leads to the change of the interface magnetization indicating a sizable magnetoelectric effect. The magnitude of the magnetoelectric effect depends on the interface termination. Two different interfaces have been studied: oxygen-rich TiO_2-$FeO_2(B)$ and oxygen-deficient TiO_2-Fe(A). We find that the effect is much stronger for the oxygen-deficient $BaTiO_3/Fe_3O_4$ interface. This is due to the bonding between Fe and Ti atoms which induces magnetic moments on the interface Ti atoms sensitive to the Fe-Ti bond length. The magnitude of the magnetic moment change per surface unit cell is predicted as large as 0.6 μ_B for the oxygen-deficient TiO_2-Fe(A) and 0.2 μ_B for the oxygen-rich TiO_2-$FeO_2(B)$ interfaces. This leads to the interface magnetoelectric coefficients of $\alpha_s \approx 2.1 \times 10^{-10}$ G cm^2/V and of $\alpha_s \approx 0.07 \times 10^{-10}$ G cm^2/V for the two interfaces, respectively. The sensitivity to the oxygen content suggests that oxidation or oxygen vacancies at the interface may play an important role in determining the strength of the coupling. The predicted magnetoelectric effect is interesting from the point of view of controlling magnetic properties by electric fields and possible multifunctional device applications.

ACKNOWLEDGMENTS

This work was supported by the Office of Naval Research, National Science Foundation, and the Nanoelectronics Research Initiative through the Materials Research Science and Engineering Center at the University of Nebraska. C.-G.D. thanks the National Science Foundation of China (Grant No. 50771072) for support. Computations were performed utilizing the Research Computing Facility of the University of Nebraska-Lincoln.

*mniranjan2@.unl.edu
†tsymbal@unl.edu

[1] W. Eerenstein, N. D. Mathur, and J. F. Scott, Nature (London) **442**, 759 (2006).
[2] M. Fiebig, J. Phys. D **38**, R123 (2005).
[3] N. A. Spaldin and M. Fiebig, Science **309**, 391 (2005).
[4] T. Kimura, T. Goto, H. Shintani, K. Ishizaka, T. Arima, and Y. Tokura, Nature (London) **426**, 55 (2003).
[5] T. Lottermoser, T. Lonkai, U. Amann, D. Hohlwein, J. Ihringer, and M. Fiebig, Nature (London) **430**, 541 (2004).
[6] P. Borisov, A. Hochstrat, X. Chen, W. Kleemann, and Ch. Binek, Phys. Rev. Lett. **94**, 117203 (2005).
[7] V. Laukhin, V. Skumryev, X. Marti, D. Hrabovsky, F. Sanchez, M. V. Garcia-Cuenca, C. Ferrater, M. Varela, U. Luders, J. F. Bobo, and J. Fontcuberta, Phys. Rev. Lett. **97**, 227201 (2006).
[8] M. Weisheit, S. Fähler, A. Marty, Y. Souche, C. Poinsignon, and D. Givord, Science **315**, 349 (2007).
[9] W. Eerenstein, M. Wiora, J. L. Prieto, J. F. Scott, and N. D. Mathur, Nat. Mater. **6**, 348 (2007).
[10] S. Sahoo, S. Polisetty, C.-G. Duan, S. S. Jaswal, E. Y. Tsymbal, and Ch. Binek, Phys. Rev. B **76**, 092108 (2007).
[11] C.-G. Duan, J. P. Velev, R. F. Sabirianov, W. N. Mei, S. S. Jaswal, and E. Y. Tsymbal, Appl. Phys. Lett. **92**, 122905 (2008).
[12] E. Y. Tsymbal and H. Kohlstedt, Science **313**, 181 (2006).
[13] M. Y. Zhuravlev, R. F. Sabirianov, S. S. Jaswal, and E. Y. Tsymbal, Phys. Rev. Lett. **94**, 246802 (2005); M. Y. Zhuravlev, S. S. Jaswal, E. Y. Tsymbal, and R. F. Sabirianov, Appl. Phys. Lett. **87**, 222114 (2005).
[14] Ch. Binek and B. Doudin, J. Phys.: Condens. Matter **17**, L39 (2005).
[15] M. Gajek, M. Bibes, S. Fusil, K. Bouzeouane, J. Fontcuberta, A. Barthelemy, and A. Fert, Nat. Mater. **6**, 296 (2007).
[16] J. P. Velev, C.-G. Duan, K. D. Belashchenko, S. S. Jaswal, and E. Y. Tsymbal, Phys. Rev. Lett. **98**, 137201 (2007); K. Janicka, J. P. Velev, and E. Y. Tsymbal, J. Appl. Phys. **103**, 07B508 (2008).
[17] I. Dzyaloshinskii, Sov. Phys. JETP **10**, 628 (1960).
[18] H. Zheng, J. Wang, S. E. Lofland, Z. Ma, L. Mohaddes-Ardabili, T. Zhao, L. Salamanca-Riba, S. R. Shinde, S. B. Ogle, F. Bai, D. Viehland, Y. Jia, D. G. Schlom, M. Wuttig, A. Roytburd, and R. Ramesh, Science **303**, 661 (2004).
[19] F. Zavaliche, H. Zheng, L. M. Ardabili, S. Y. Yang, Q. Zhan, P. Shafer, E. Reilly, R. Chopdekar, Y. Jia, P. Wright, D. G. Schom, Y. Suzuki, and R. Ramesh, Nano Lett. **5**, 1793 (2005).
[20] D. Dale, A. Fleet, J. D. Brock, and Y. Suzuki, Appl. Phys. Lett. **82**, 3725 (2003).
[21] M. K. Lee, T. K. Nath, C. B. Eom, M. C. Smoak, and F. Tsui, Appl. Phys. Lett. **77**, 3547 (2000).
[22] R. V. Chopdekar and Y. Suzuki, Appl. Phys. Lett. **89**, 182506 (2006).
[23] H. F. Tian, T. L. Qu, L. B. Luo, J. J. Yang, S. M. Guo, H. Y. Zhang, Y. G. Zhao, and J. Q. Li, Appl. Phys. Lett. **92**, 063507 (2008).
[24] C.-G. Duan, S. S. Jaswal, and E. Y. Tsymbal, Phys. Rev. Lett. **97**, 047201 (2006).
[25] J. M. Rondinelli, M. Stengel, and N. A. Spaldin, Nat. Nanotechnol. **3**, 46 (2008).
[26] K. Yamauchi, B. Sanyal, and S. Picozzia, Appl. Phys. Lett. **91**, 062506 (2007).
[27] M. Bibes and A. Barthelemy, IEEE Trans. Electron Devices **54**, 1003 (2007).
[28] S. Lee, A. Fursina, J. T. Mayo, C. T. Yavuz, V. L. Kolvin, R. G. S. Sofin, I. G. Shvets, and D. Natelson, Nat. Mater. **7**, 130 (2008).
[29] J. M. D. Coey and C. L. Chien, MRS Bull. **28**, 720 (2003).
[30] Z.-M. Liao, Y.-D. Li, J. Xu, J.-M. Zhang, K. Xia, and D. Yu, Nano Lett. **6**, 1087 (2006).
[31] Y. C. Sui, R. Skomski, K. D. Sorge, and D. J. Sellmyer, Appl. Phys. Lett. **84**, 1525 (2004).
[32] M. Matsubara, Y. Shimada, T. Arima, Y. Taguchi, and Y. Tokura, Phys. Rev. B **72**, 220404(R) (2005).

[33] G. T. Rado and J. M. Ferrari, Phys. Rev. B **15**, 290 (1977).
[34] E. J. W. Verwey, Nature (London) **144**, 327 (1939).
[35] F. Walz, J. Phys.: Condens. Matter **14**, R285 (2002).
[36] J. Garcia and G. Subias, J. Phys.: Condens. Matter **16**, R145 (2004).
[37] E. Nazarenko, J. E. Lorenzo, Y. Joly, J. L. Hodeau, D. Mannix, and C. Marin, Phys. Rev. Lett. **97**, 056403 (2006).
[38] W. Kohn and L. J. Sham, Phys. Rev. **140**, A1133 (1965).
[39] P. E. Blöchl, Phys. Rev. B **50**, 17953 (1994).
[40] G. Kresse and J. Furthmuller, Phys. Rev. B **54**, 11169 (1996).
[41] J. P. Perdew, K. Burke, and M. Ernzerhof, Phys. Rev. Lett. **77**, 3865 (1996).
[42] H. J. Monkhorst and J. D. Pack, Phys. Rev. B **13**, 5188 (1976).
[43] P. Morrall, F. Schedin, S. Langridge, J. Bland, M. F. Thomas, and G. Thornton, J. Appl. Phys. **93**, 7960 (2003).
[44] Z. Zhang and S. Satpathy, Phys. Rev. B **44**, 13319 (1991).
[45] M. Fonin, Yu. S. Dedkov, R. Pentcheva, U. Rudiger, and G. Guntherodt, J. Phys.: Condens. Matter **19**, 315217 (2007).
[46] P. A. Dowben and R. Skomski, J. Appl. Phys. **95**, 7453 (2004).
[47] P. Piekarz, K. Parlinski, and A. M. Oles, Phys. Rev. Lett. **97**, 156402 (2006).
[48] H.-T. Jeng, G. Y. Guo, and D. J. Huang, Phys. Rev. Lett. **93**, 156403 (2004).
[49] I. Leonov, A. N. Yaresko, V. N. Antonov, M. A. Korotin, and V. I. Anisimov, Phys. Rev. Lett. **93**, 146404 (2004).
[50] A. I. Liechtenstein, V. I. Anisimov, and J. Zaanen, Phys. Rev. B **52**, R5467 (1995).
[51] I. I. Oleinik, E. Y. Tsymbal, and D. G. Pettifor, Phys. Rev. B **65**, 020401(R) (2001).
[52] J. Junquera and P. Ghosez, Nature (London) **422**, 506 (2003).
[53] N. Sai, A. M. Kolpak, and A. M. Rappe, Phys. Rev. B **72**, 020101(R) (2005).
[54] Y. Umeno, B. Meyer, C. Elsässer, and P. Gumbsch, Phys. Rev. B **74**, 060101(R) (2006).
[55] C.-G. Duan, R. F. Sabirianov, W.-N. Mei, S. S. Jaswal, and E. Y. Tsymbal, Nano Lett. **6**, 483 (2006).
[56] G. Gerra, A. K. Tagantsev, and N. Setter, Phys. Rev. Lett. **98**, 207601 (2007).
[57] C.-G. Duan, J. P. Velev, R. F. Sabirianov, Z. Zhu, J. Chu, S. S. Jaswal, and E. Y. Tsymbal (unpublished).
[58] N. Berdunov, S. Murphy, G. Mariotto, and I. V. Shvets, Phys. Rev. Lett. **93**, 057201 (2004).